MATERIALS CHEMISTRY FRONTIERS

RESEARCH ARTICLE

View Article Online
View Journal | View Issue

Cite this: *Mater. Chem. Front.*, 2023, **7**, 1671

An electrical microenvironment constructed based on electromagnetic induction stimulates neural differentiation

Fangwei Qi,[ab] Ruobing Liao,[a] Ping Wu,[c] Huixing Li,[a] Jun Zan,[a] Shuping Peng *[de] and Cijun Shuai *[af]

Electrical stimulation is considered an effective way to accelerate peripheral nerve cell growth. However, reliance on external wires and a power supply restricts its further applications. In this work, a wireless magnet-powered electrical stimulation system was constructed based on the electromagnetic induction effect. Specifically, amino-functionalized conductive MXene nanosheets were first wrapped on the PLLA particles' surface by electrostatic assembly. Then the conductive NH_2-MXene/PLLA conduit was fabricated by laser additive manufacturing. Triggered by a rotating magnetic field, the conduit could act as a coil to cut magnetic induction lines, converting magnetic energy into electrical energy and thereby achieving wireless electrical stimulation. The results indicate that the conduit presented an excellent conductivity of 8.44 S m^{-1}, benefiting from its formed conductive network structure. Under excitation of the rotating magnetic field, the conduit generated an electric current of 10 μA, which is in the appropriate range for nerve cell growth. An *in vitro* cell test confirmed that the generated current effectively enhanced the PC12 cell proliferation, neurite growth and differentiation-related mRNA (Nestin, MAP2 and Tuj1) expression. Moreover, it also promoted PC12 cells to differentiate into mature neurons, evidenced by calcium sparks produced in PC12-derived neurons. Collectively, this wireless electrical stimulation system offers a new perspective on peripheral nerve repair.

Received 18th November 2022,
Accepted 28th February 2023

DOI: 10.1039/d2qm01193j

rsc.li/frontiers-materials

1. Introduction

Electrical stimulation was regarded as pivotal to promoting peripheral nerve cell growth, which could enhance cell proliferation and axon regeneration by regulating ion flux and signal transduction.[1,2] However, the current electrical stimulation methods rely on an external power supply to provide electrical signals and complicated wiring to transmit the electrical signals against cells.[3–5] This was not only quite uncomfortable and inconvenient in actual application, but also required additional surgery to remove wires after treatment, leading to secondary damage.

Recently, implanting devices capable of performing wireless electrical stimulation has attracted considerable attention in nerve repair.[6–9] For instance, Tang *et al.*[10] developed a wireless light-powered scaffold based on an optoelectronic effect to modulate neuronal cell behavior. In another study, Cheng *et al.*[11] prepared a wireless self-powered nerve tissue engineering scaffold composed of PVDF and PCL to stimulate nerve regeneration. Although these studies achieved great success in constructing a wireless electrical stimulation device for nerve repair, their preparation was either complex or the generated electric current intensity was uncontrollable.

It was well established that the conductive coil could generate an induced electric current when the passing magnetic flux changed, which is the famous Faraday electromagnetic induction law.[12] Inspired by this, we envisaged constructing a conductive nerve conduit and then placing it in a variable magnetic field (MF) provided by a rotating magnet. The conduit would act as a coil to cut the magnetic induction line, converting magnetic energy into electrical energy and thus realizing wireless electrical stimulation. More importantly, the generated

[a] *Institute of Bioadditive Manufacturing, Jiangxi University of Science and Technology, Nanchang, 330013, China. E-mail: shuai@csu.edu.cn*
[b] *State Key Lab of Polymer Materials Engineering, Polymer Research Institute, Sichuan University, Chengdu, 610065, China*
[c] *School of Traditional Chinese Medicine, Hunan University of Chinese Medicine, Changsha, Hunan 410208, China*
[d] *NHC Key Laboratory of Carcinogenesis, The Key Laboratory of Carcinogenesis and Cancer Invasion of the Chinese Ministry of Education, School of Basic Medical Science, Central South University, Changsha, 410078, Hunan, China. E-mail: shuping@csu.edu.cn*
[e] *School of energy and machinery engineering, Jiangxi University of Science and Technology, Nanchang 330013, China*
[f] *State Key Laboratory of High Performance Complex Manufacturing, Central South University, Changsha 410083, China*

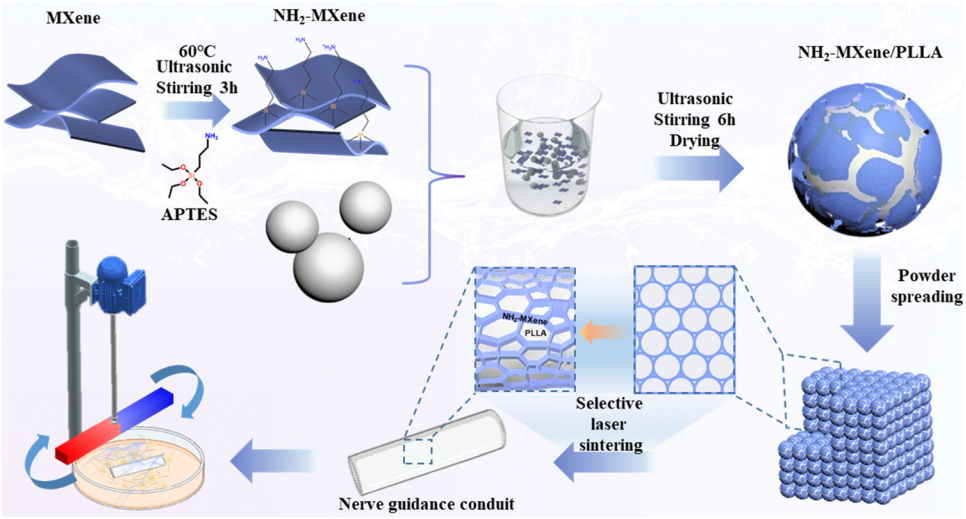

Fig. 1 The schematic illustration of nerve guidance conduit fabrication.

electric current intensity could be controlled by regulating the rotation speed of the magnet.

In this work, $Ti_3C_2T_x$ (MXene) nanosheets, which exhibit excellent electrical performance,[13,14] were first amino-functionalized and then wrapped on the poly-L-lactic acid (PLLA) particles' surface through electrostatic assembly (Fig. 1). Subsequently, the conductive NH_2-MXene/PLLA nerve conduit with a conductive network structure was prepared through laser additive manufacturing. Finally, the conduit was co-cultured with PC12 cells under a rotating MF, aiming to generate wireless electrical signals to stimulate cell differentiation. The morphology and physicochemical properties of the powders were thoroughly investigated. The induced electric current intensity of conduits under a rotating MF with various rotating speeds was evaluated. The magnetic-electrical conversion was simulated using COMSOL software. The effect of electric stimulation on cell proliferation, differentiation, and differentiation-related mRNA expression was investigated. Moreover, the function expression of PC12-derived neurons was detected. This work not only provides a new wireless electric stimulation strategy for accelerating nerve cell differentiation, but also expands the application of electromagnetic induction in nerve regeneration.

2. Experimental section

2.1. Materials

PLLA was supplied by Shenzhen Polymtek Biomaterial Co., Ltd. (Shenzhen, China). $Ti_3C_2T_x$ MXene was provided by beike 2D materials Co., Ltd. (Beijing, China). In addition, 3-aminopropyltriethoxysilane ($C_9H_{23}NO_3Si$, APTES) was obtained from J & K Scientific Ltd. (Beijing, China), γ-aminobutyric acid (GABA) was purchased from Beyotime Biotechnology Co., Ltd. (Shanghai, China) and dopamine (DA) was provided by Aladdin Biochemical Technology Co., Ltd (Shanghai, China).

2.2. Synthesis of NH_2-MXene

A schematic diagram of the MXene amination process is displayed in Fig. 1. Briefly, 5 parts by weight of APTES were added to 100 parts by weight of ethanol aqueous solution (volume ratio of ethanol and water : 95 : 5), then stirred evenly, then 20 parts by weight of MXene were added, dispersed evenly by ultrasonication, and heated up and stirred at 60 °C for 3 h. Finally, the amino-modified MXene (labeled as NH_2-MXene) was obtained after three washings and 24 h of drying at 60 °C.

2.3. Preparation of NH_2-MXene/PLLA nerve conduit

Designed mass ratio NH_2-MXene and PLLA powders were first weighed and mixed in beakers with 20 mL of deionized water. After that, the suspension was agitated and sonicated simultaneously for 6 h. A composite powder was created by filtering, drying, and grinding the material. Lastly, laser additive manufacturing equipment was used to create the guide conduit, utilizing 0.6 W laser power, 200 mm s^{-1} scanning speed, 0.08 mm incubation distance, and 0.1 mm single-layer thickness. The prepared conduits were denoted as NH_2-MXene-1, NH_2-MXene-2 and NH_2-MXene-3, which represented 5 wt%, 10 wt% and 15 wt% NH_2-MXene in conduits, respectively.

2.4. Analysis and characterization

Scanning electron microscopy (SEM, Zeiss, Germany) and transmission electron microscopy (TEM, FEI, USA) were used to identify the morphologies and elemental distribution of the samples. X-ray photoelectron spectroscopy (XPS, Thermo-VG Scientific Ltd., UK) was used to assess the chemical composition of samples. Zeta potential measurements (Malvern Zetasizer Nano ZS90, UK) were performed on the samples redispersed in water by sonication for 30 min.

2.5. Conductivity

The conductivity of the conduits was measured by the linear four-probe method by placing electrodes of the 34401 A

multimeter on the two sides of the sample. The samples' conductivity (σ) was determined using eqn (1)

$$\sigma = L/(A \times R) \quad (1)$$

where A represents the cross-sectional area (1 mm^2) and L represents the length (4 mm).

2.6. Wireless electrical stimulation

Using Faraday's law of electromagnetic induction and a self-made 0–400 revolutions per minute (RPM) rotating magnet (0.6 T) in conjunction with a nerve conduit, the wireless electrical stimulation-assisted neural differentiation system was constructed.

2.7. Culture of PC12 cells

Rat pheochromocytoma (PC12) cells were chosen as the model cell because they are commonly employed in *in vitro* neural regeneration research and could be differentiated into neuron-like cells. Before cell seeding, all conduits were disinfected in a 48-well plate with 75% ethanol (1 mL per well) and a strong UV light. After sterilization, the samples were washed three times with sterile PBS. Then, in the aforementioned 48-well plate, undifferentiated PC12 cells (Procell Life Science & Technology Co., Ltd., Wuhan, China) were seeded at a density of 4×10^3 cells per well using RPMI-1640 medium supplemented with 10% heat-inactivated horse serum, 5% fetal bovine serum, 100 μg mL^{-1} penicillin, and 100 μg mL^{-1} streptomycin. Subsequently, different nerve conduits were placed into the plate and culture plates were put in this wireless electrical stimulation device for 15 min every day.

2.8. Biocompatibility of the NH_2-MXene/PLLA conduit

After 5 days of co-culture, the conduits were taken out and the cells were digested with trypsin. Then, the digested cells were collected in the plate and stained with calcein/PI (Live/Dead, Beyotime, Shanghai, China) and cultured for another 30 min. Following that, the labeled cells were rinsed three times with PBS. Finally, the cells were examined under a fluorescent microscope (Olympus Co. Ltd., Tokyo, Japan).

A CCK-8 test was used to quantitatively examine cell proliferation behavior. After 1, 3, and 5 days of culture, the cells were trypsin digested and then fixed in PBS with 4% paraformaldehyde for 15 min. The CCK-8 solution (Beyotime, Shanghai, China) was diluted 1 : 10 with medium before being cultured with cells in a 37 °C incubator for 2 h. Following that, the medium from each well was collected for additional OD value measurements at 450 nm using a multifunction microplate scanner (TECAN infinite M200, Taunton, MA, USA).

2.9. Neural differentiation of PC12 cells *in vitro*

The cell-conduit complex was collected from the medium and rinsed with PBS solution after culturing for 1 day under normal conditions. Then the complex was transferred to the new medium containing nerve growth factor (NGF, Cloud-clone corp., Wuhan, China, 100 ng mL^{-1}) and the culture continued in a constant temperature incubator at 37 °C. The medium was changed every two days. After 5 days of culture, the conduits were taken out and the cells were digested with trypsin. Then, the digested cells were collected in the plate and differentiation was observed using an inverted microscope. Additionally, the neurite length was quantified using ImageJ software.

2.10. Real-time qPCR

To convert mRNA to cDNA, reverse transcription was performed using a first-strand cDNA synthesis kit after the certain time of differentiation. Following that, quantitative polymerase chain reaction (qPCR) was performed and monitored in a 7500 Real-time PCR machine using PowerUp SYBR Green Master Mix (Applied Biosystems, Thermo Fisher Scientific, USA). Nestin, Tuj1, and MAP2 were selected for testing. Nestin is an intermediate filament protein that is found mostly in nerve cells and is linked to axon radial expansion. MAP2 is a neuronal phosphoprotein that is required for neuronal morphological and functional differentiation. Tuj1 is tubulin that aids in the development of neurons' neurites. Sangon Biotech (Shanghai, China) provided the primers for Nestin, Tuj1, and MAP2 for qPCR. To normalize the expression levels, β-actin was utilized as a reference gene, and the results were computed using the $2^{-\Delta\Delta Ct}$ technique.

2.11. Intracellular calcium measurement

After 5 days of co-culture of the conduit and cell, the conduits were taken out and the cells were digested with trypsin. Then, the cells were washed with PBS three times, and 2 μM Ca^{2+}-sensitive indicator Fluo-4 AM (Sangon Biotech, China) was added into the medium for 30 min at 37 °C. After washing the cells with PBS, fluorescence pictures were monitored using a fluorescence microscope. γ-aminobutyric acid (GABA) solution and dopamine (DA) solution (0.5 m) were selected as experimental neurotransmitters and 100 μL of them were dripped during the experiment. The fluorescence changes ($\%\Delta F/F_0$) were calculated using the formula $\Delta F/F_0 = (F_1 - F_0)/F_0 \times 100\%$, where F_1 was the fluorescence of the cell after stimulation, and F_0 was the fluorescence of the cell before stimulation.

3. Results and discussion

3.1. NH_2-MXene characterization

The morphology of MXene and NH_2-MXene was measured using TEM, as displayed in Fig. 2a and b. Original MXene has a sheet-like structure with an average size of ~80 nm, whereas NH_2-MXene exhibited a similar sheet structure, which indicated the incorporation of amine groups did not cause damage to the structure of MXene.[15,16] Corresponding elemental distribution (Fig. 2c–f) confirmed the successful preparation of NH_2-MXene, as evidenced by the simultaneous presence of C and Ti elements of MXene and N elements of APTES.[17–19]

The chemical composition of NH_2-MXene was investigated *via* XPS, as shown in Fig. 2g and h. Obviously, the bonding orbitals of C1s, N1s and Ti2p belonging to NH_2-MXene were observed, indicating the successful grafting of amine groups

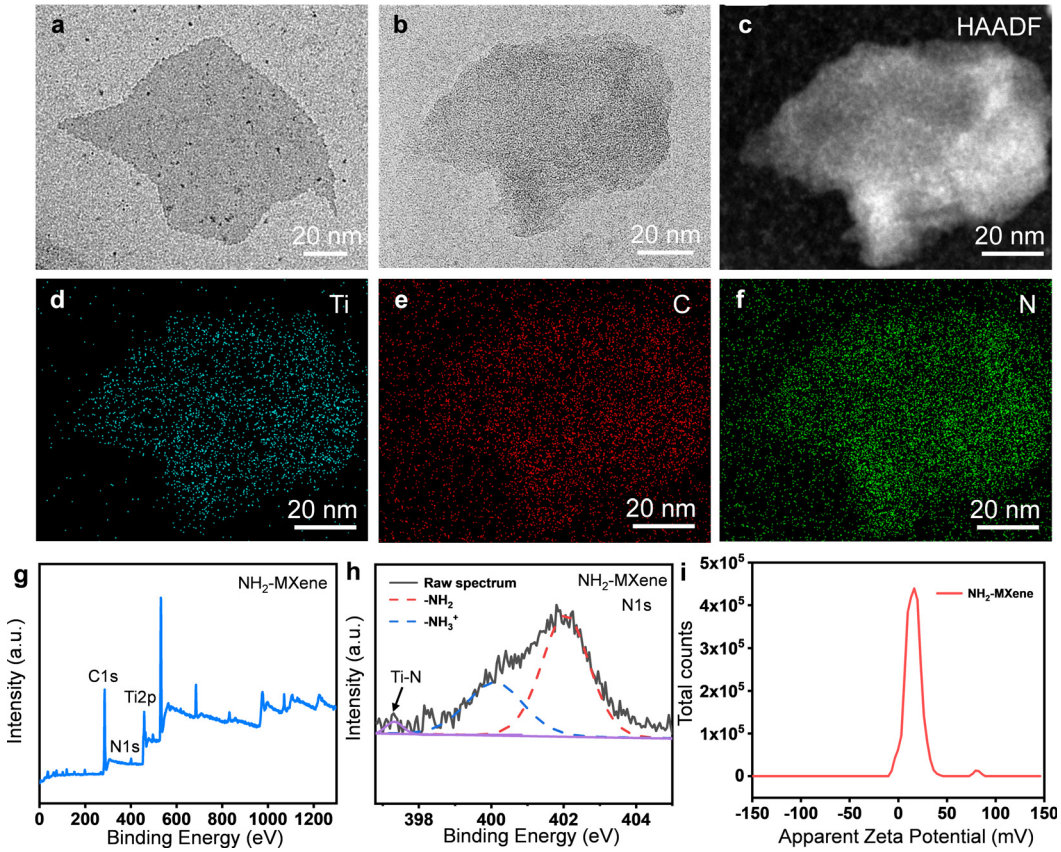

Fig. 2 TEM images of (a) MXene and (b) NH_2-MXene; (c–f) EDS maps of the NH_2-MXene; (g) XPS wide-scan spectra, (h) high-resolution XPS spectra of N1s core and (i) surface charge of NH_2-MXene.

(Fig. 2g).[20] The existing form of amine groups was further analyzed using the N1s high-resolution XPS spectrum, as displayed in Fig. 2h. Two obvious peaks occurring at 400.2 and 402.1 eV were observed, which correspond to free ($-NH_3^+$) and protonated amines ($-NH_2$), respectively.[21] In addition, the presence of Ti–N (~397.3 eV) might be due to the condensation reaction between the amine group of APTES and the hydroxyl group.[22] Considering the positive charge of the amine groups, the zeta potential of NH_2-MXene was analyzed, as displayed in Fig. 2i. Clearly, the zeta potentials of NH_2-MXene were concentrated in the positive region and its mean potential reached 15.2 mV, thus further confirming the presence of amine groups on the outer surface of MXene.[23,24]

3.2. Synthesis and characterization of NH_2-MXene/PLLA powders

NH_2-MXene/PLLA was prepared by ultrasonic assistance, and the corresponding morphology is shown in Fig. 3a–c. Clearly, the color of NH_2-MXene/PLLA exhibited no obvious change compared to NH_2-MXene, and both appeared black (Fig. 3a). It can be seen from the SEM images in Fig. 3b and c that the surface of the PLLA particle was smooth, while the surface of the NH_2-MXene/PLLA particle was relatively rough. Further analysis of the EDS spectra of the NH_2-MXene/PLLA particle at point I, II and III (Fig. 3d), showed the N and Ti elements belonging to NH_2-MXene appeared, and it could be assumed that NH_2-MXene sheets were wrapped around the PLLA particles' surface *via* electrostatic assembly.

The zeta potentials of MXene, NH_2-MXene and PLLA were studied, as shown in Fig. 3e. The average zeta potentials of the original MXene and PLLA were −45.5 mV and −35.3 mV, respectively. The results were attributed to the negative charge of hydroxyl and carboxyl groups on their surfaces.[25] In contrast, the zeta potential of NH_2-MXene powder was 14.9 mV, which was attributed to its amine groups.[24] For the original MXene, it could only be combined with PLLA through weak van der Waals forces. For NH_2-MXene, it had a positive zeta potential, which could form strong electrostatic interaction with negative PLLA and thus enhance their binding effect.[26] Importantly, the average zeta potentials of NH_2-MXene-1, NH_2-MXene-2 and NH_2-MXene-3 were −18.4 mV, 14.3 mV and 16.5 mV, respectively. The zeta potential value of NH_2-MXene/PLLA suddenly changes from negative to positive with the increase of NH_2-MXene content. These results could indicate that NH_2-MXene was completely assembled on the PLLA surface owing to the electrostatic interaction between the oppositely charged materials.[27]

To further confirm this electrostatic adsorption, the FTIR spectrum of NH_2-MXene/PLLA was detected, as displayed in Fig. 3f. Two new peaks at 3612 and 3419 cm^{-1} were observed

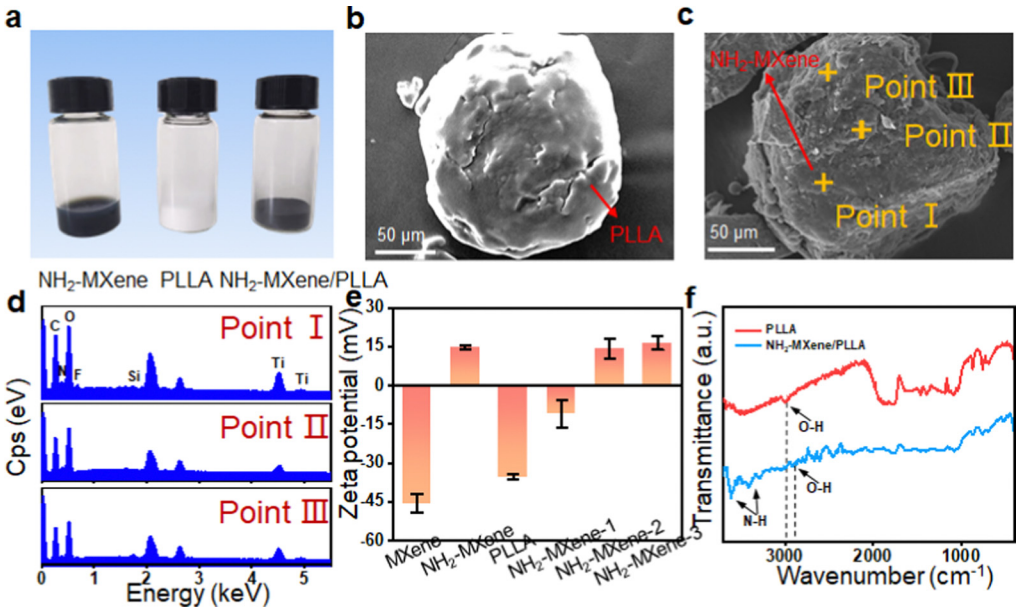

Fig. 3 (a) Digital photos of NH_2-MXene, PLLA and NH_2-MXene/PLLA; SEM image of (b) PLLA and (c) mixed powder; (d) the EDS spectrums of mixed powder in point I, II and III; (e) Zeta potential of MXene, NH_2-MXene, PLLA, NH_2-MXene-1, NH_2-MXene-2 and NH_2-MXene-3; (f) FTIR spectrum of PLLA and NH_2-MXene/PLLA.

after the introduction of NH_2-MXene, which were attributed to the bending vibrations of N–H.[28] More importantly, the peak position of the O–H peak in PLLA powder shifted from 3002 cm^{-1} to 2902 cm^{-1} after the introduction of NH_2-MXene. This phenomenon might be due to the fact that the electrostatic adsorption between PLLA and NH_2-MXene reduced the bonding electron cloud density.[29,30]

3.3. Characterization of nerve guidance conduit

To obtain conductor devices that generate induced electric currents, a conductive NH_2-MXene/PLLA nerve conduit was fabricated by laser additive manufacturing. The detailed laser additive manufacturing process was demonstrated as follows. Firstly, the powder was preheated to a temperature lower than its melting point, and then the powder was flattened under the action of a scraper. Subsequently, the laser beam selectively sintered the powder under the control of the computer. Eventually, the conduits were rapidly manufactured with any complex structure through layer-by-layer stacking.[31–34] As shown in Fig. 4a, clearly, the conduit presented a tubular structure with a channel diameter of 1.5 mm, which met the requirements of normal nerves.[35] The cross-section images of the conduit showed that NH_2-MXene was dispersed preferentially in the interfacial area between adjacent PLLA particles and formed a network structure (Fig. 4b). This was ascribed to the unique zero shear force and restricted flow formation characteristics of laser additive manufacturing technology, which allowed the conductive network to retain its original structure in the matrix.[36]

The LED illumination test was performed to visually check the conductivity of the conduits, as shown in Fig. 4c. Evidently, the LED indication was clearly illuminated after connecting the power supply and NH_2-MXene/PLLA conduit, which proved its good conductivity.[37] Moreover, the conduit's conductivity with different NH_2-MXene content was quantified by the linear four-probe method, as shown in Fig. 4d. The original PLLA conduit demonstrated insulating characteristics with a conductivity of 8.7×10^{-13} S m^{-1}. The conductivity of NH_2-MXene/PLLA was markedly greater than that of PLLA, indicating its good conductive properties. The significantly enhanced conductivity was attributed to the formed network structure, which could provide a continuous and efficient conductive pathway for charge transfer.[38–41] Besides, the conductivity of the conduit presented an increasing tendency as the NH_2-MXene concentration increased. Specifically, the conductivity of the NH_2-MXene-1, NH_2-MXene-2 and NH_2-MXene-3 was 9.87×10^{-5} S m^{-1}, 8.44 S m^{-1} and 32.96 S m^{-1}, respectively. According to our knowledge, the most suitable conductivity range for neural cell growth was 1–10 S m^{-1}.[42] Hence, the NH_2-MXene-2 conduit was well suited to the requirements.

To investigate the electromagnetic-induction capability of conduits and whether NH_2-MXene could convert magnetic energy into electricity, an NH_2-MXene/PLLA conduit was placed beneath a rotating MF to simulate the process of cutting magnetic induction lines (Fig. 4e). During the rotating MF application, no obvious current or voltaic changes were detected on the PLLA, whereas a significant alternating current and voltage was detected on the NH_2-MXene/PLLA conduit (Fig. 4f–i). Additionally, the magnitude of the voltage or current on NH_2-MXene/PLLA varied with the different rotating speeds. Specifically, when the speed changed from 100 rpm to 300 rpm, the current was increased from 2 to 10 μA and the voltage was increased from 0.07 to 0.21 mV. These results were consistent with our previous assumptions, thus confirming that the

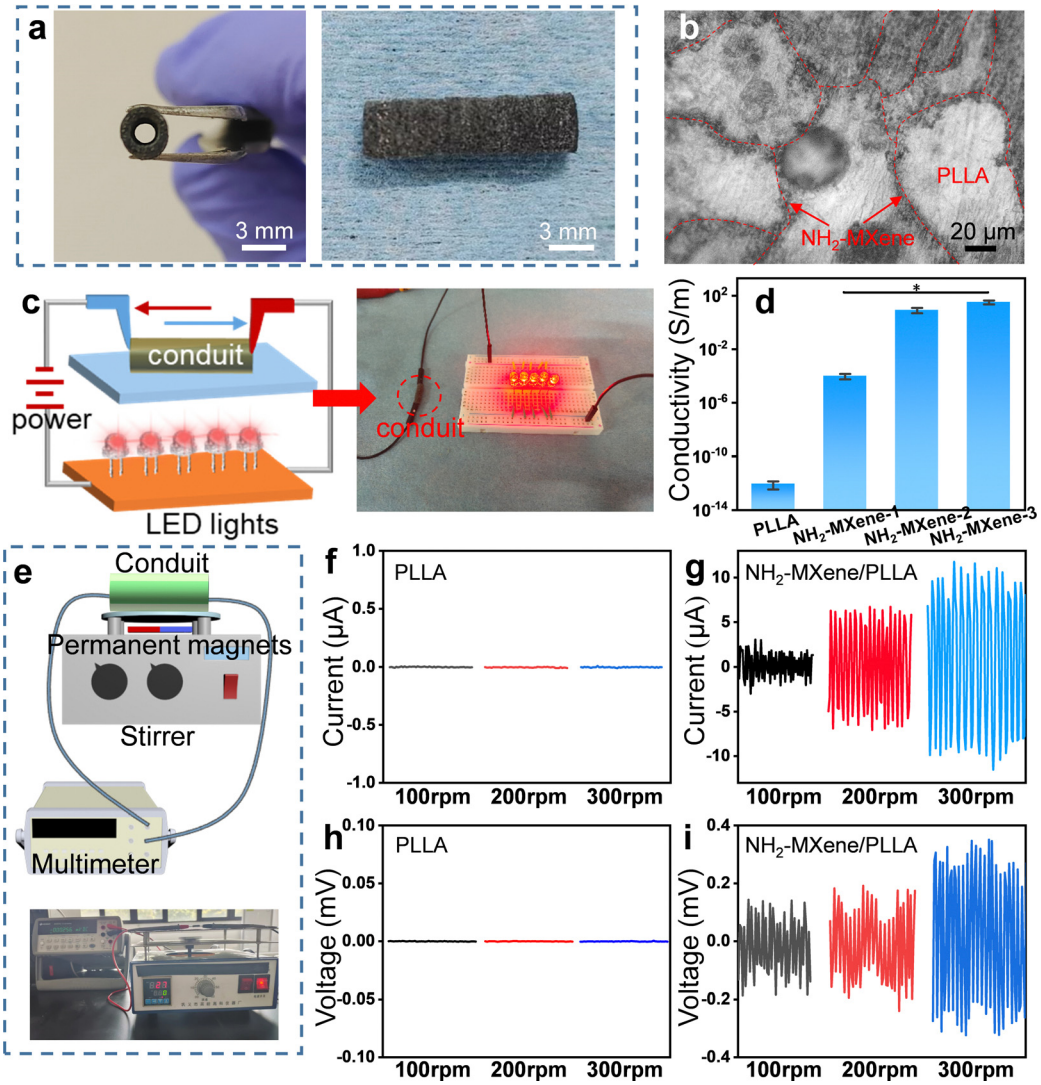

Fig. 4 (a) Optical photograph of nerve guidance conduit; (b) optical microscopic image of the conduit; (c) schematic diagram of the display of LED with conduits connected to the circuit and LED lighting experiment of conduit; (d) conductivities of the conduits; (e) schematic diagram of the electromagnetic induction detection device; the generated induced electric currents of (f) PLLA and (g) NH_2-MXene/PLLA, the generated induced voltage of (h) PLLA and (i) NH_2-MXene/PLLA.

conduit containing NH_2-MXene could be used as a conductor medium to convert enough magnetic energy into electrical energy by an electromagnetic induction effect.

3.4. Comsol simulation

Comsol simulation was used to analyze the convert relationship between magnetic energy and electrical energy. Fig. 5a and b show the permanent magnet's magnetic induction line and intensity distribution, respectively. It found that the magnetic induction lines at both ends of the permanent magnet were most densely distributed, which meant that these sites presented the largest magnetic induction intensity. Subsequently, the conduit was placed in a MF generated by the permanent magnet, with a vertical distance below the permanent magnet (Fig. 5c). As the vertical distance increased, the magnetic induction intensity decreased (Fig. 5d). To simulate the mean distance from skin to the peripheral nerve (45 ± 10 mm), the distance from the magnet to the conduit was set as 5 cm in this work.[43] As shown in Fig. 5e, the permanent magnet generated the magnetic induction lines and part of the magnetic induction line passed through the conduit. After applying 300 rpm to the magnet, the magnetic induction intensity through the conduit changed (Fig. 5f), and was displayed as a sine wave with a period of 0.2 s.

According to Faraday's law of electromagnetic induction by the following equation:

$$I = -\frac{n}{R}\frac{\Delta\phi}{\Delta t} = -\frac{nS}{R}\frac{\Delta B}{\Delta t} \quad (2)$$

where n represents the number of turns, S represents the sectional area of the magnetic circuit, R represents the resistance of the conduit, and $\Delta B/\Delta t$ represents the change rate of magnetic induction intensity.[44] Theoretically, the induced

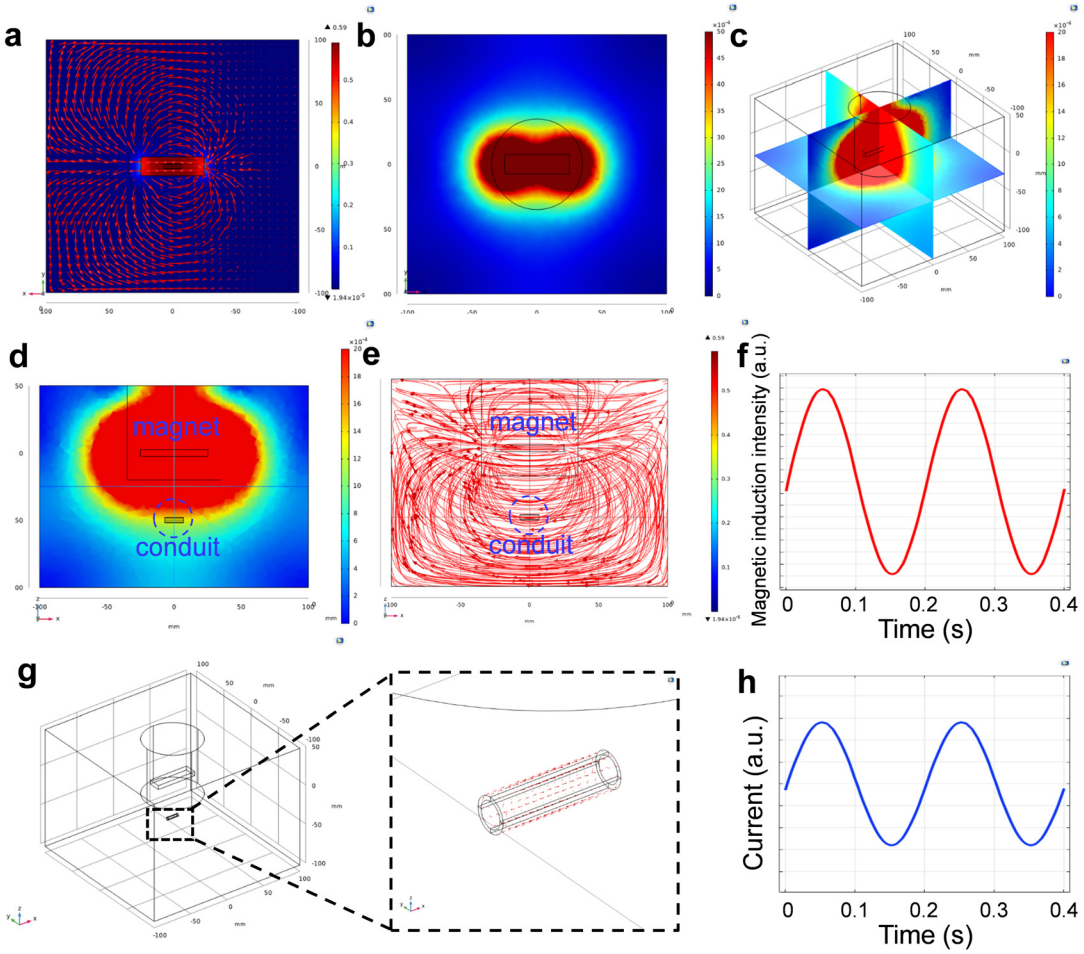

Fig. 5 (a) Top view of simulated magnetic induction lines of induction generated by a permanent magnet; (b) top view of the tangential distribution of the magnetic induction intensity produced by the permanent magnets; (c) spatial distribution of the magnetic induction intensity produced by the permanent magnets; (d) side view of the spatial distribution of the magnetic induction intensity produced by a permanent magnet; (e) side view of the spatial distribution of magnetic induction lines produced by a permanent magnet; (f) magnetic induction intensity of conduit section at 300 rpm; (g) side view of the induced electric current generated by the conduit, in which red arrows represented current and (h) induced electric current generated by the conduit under rotating magnetic field at 300 rpm.

electric current would be generated when the magnetic flux through the conduit changed. In fact, when the permanent magnet rotated, an electric current was generated on the conduit (Fig. 5g). By analyzing the current generated (Fig. 5h), the change frequency of the current was exactly the same as the change frequency of magnetic induction intensity, which was consistent with eqn (2). The above results proved that the current generated by the conduit was caused by the change in the magnetic flux passing through the conductor, and the frequency could be controlled by adjusting the rotating speed.

3.5. Cell proliferation and cytotoxicity

Previous research reported that intermittent current stimulation with 10 μA could provide a relatively comfortable environment to promote the growth of nerve cells.[45] Combing the above results (Fig. 4g), rotating MF with a speed of 300 rpm was selected to treat the cell-conduit complex. The biocompatibility of nerve cells incubated on the nerve conduits was tested by live/dead fluorescence staining, as shown in Fig. 6a. Obviously, the majority of cells for all samples were viable, indicating their good biocompatibility.[46–49] Moreover, the number of living cells on NH_2-MXene/PLLA groups excited by rotating MF was higher than that on the rest of the groups, which was attributed to the generated electrical signal promoting the nerve cell growth.[50,51]

The CCK-8 assay was employed to quantificationally analyze cell proliferation, as shown in Fig. 6b. It was seen that the OD values for all samples increased in a time-dependent manner. After culture for 5 days, the OD value of the NH_2-MXene/PLLA groups was significantly higher than that of the PLLA groups under the same conditions, which was consistent with the above live/dead fluorescent staining results. Importantly, the OD value of the NH_2-MXene/PLLA groups increased from 2.27 to 2.53 after applying the rotating MF, which proved that the NH_2-MXene/PLLA conduit could better promote cell proliferation under a rotating MF.[52,53] Similarly, the cell viability test showed the NH_2-MXene/PLLA group under a rotating MF had the best promoting impact on cell growth (Fig. 6c).

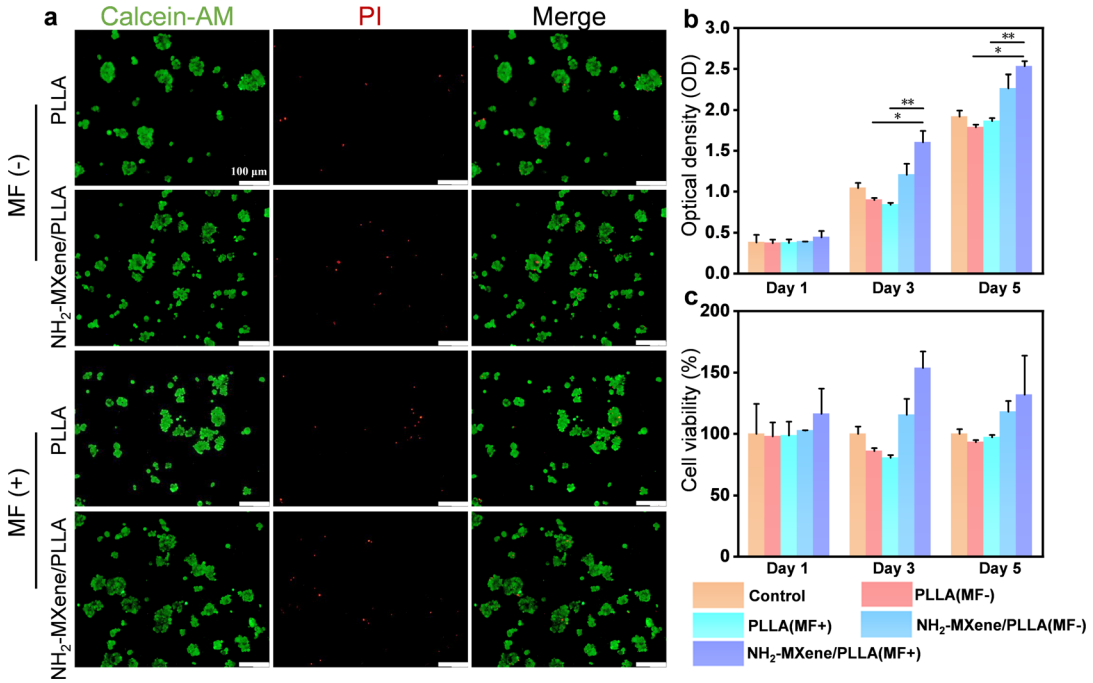

Fig. 6 (a) Cells stained by calcein-AM (green, live cells) and propidium iodide (red, dead cells) on different substrates at day 5, where MF (+) represents with MF treatment, MF (−) represents without MF treatment; (b) CCK-8 analysis; (c) cell viability. *$p < 0.05$, **$p < 0.01$.

3.6. Cell differentiation

It was well established that the regeneration of a defective nerve was accompanied by nerve cell differentiation and neurite extension, which reflected the conduits' ability to repair nerves.[54] The morphology of cell differentiation on the different substrates at 5 days was studied, as displayed in Fig. 7a. Among them, undifferentiated PC12 cells were round cells with a halo and differentiated cells became the shape of sympathetic neurons and grew neurites.[55] By analyzing neurite outgrowth, it could be found that cells on all groups had neurite, and the cells cultured in NH_2-MXene/PLLA under a rotating magnetic field possessed the longest neurite, indicating its excellent differentiation performance.[56] The percentage and neurite length of differentiated PC12 were determined from optical images. The percentages of sympathetic neuron-like cells with neurites in the NH_2-MXene/PLLA groups significantly increased under the same conditions, in comparison with that of the other two groups (Fig. 7b). In particular, the percentage of sympathetic neuron-like cells with neurites in the NH_2-MXene/PLLA (MF−) group increased from around 13.4% to 30.6%, as compared with that of the control (MF−) group. More significantly, the percentage of sympathetic neuron-like cells with neurites reached 93.1% after applying a rotating MF. The average length of neurite reflected a similar trend to the percentage of differentiation (Fig. 7c). The average length of neurite in the NH_2-MXene/PLLA (MF+) group was higher than that of other groups, reaching 32.9 μm. The results indicated that the electric current generated by the NH_2-MXene/PLLA conduit mediated through rotating MF could promote differentiation of PC12 cells.[57,58] In addition, NH_2-MXene endowed the conduit with favorable conductivity, which could also promote nerve cell differentiation through the recovery of electrical signals transmission and regulation of nerve cell membrane function.[59]

3.7. mRNA expression

qPCR was performed to quantitatively detect the expression of differentiation-related mRNA. In this work, Nestin, MAP2 and Tuj1 as representative mRNA were examined to assess the differentiation of PC12 cells. As shown in Fig. 8, the mRNA level of Nestin, MAP2 and Tuj1 did not differ significantly in the presence or absence of MF after PC12 was co-cultured with PLLA conduit for 5 days and 10 days, demonstrating that MF had no obvious influence on the differentiation of PC12 cells on the PLLA groups. Additionally, the expression of Nestin in the NH_2-MXene/PLLA group without MF was slightly upregulated at 5 days, which benefited from a conductive substrate that promoted cell differentiation.[60] Astonishingly, the expression of Nestin was upregulated 9.2-fold in cells cultivated on NH_2-MXene/PLLA using the treatment of rotating MF for 5 days (Fig. 8a), which was entirely different from that on PLLA under the same culture conditions.

On the 10th day, the mRNA expression of Nestin in the cells cultured on NH_2-MXene/PLLA under rotating MF was maintained at 46.09 (Fig. 8b), which was remarkably higher than that of the control groups. Significantly, cells on NH_2-MXene/PLLA with the administration of a rotating MF displayed a higher expression of MAP2 and Tuj1 compared with those cultured on other groups (Fig. 8c–f). High expression levels of Nestin, MAP2 and Tuj1 indicated that the electrical stimulation generated by

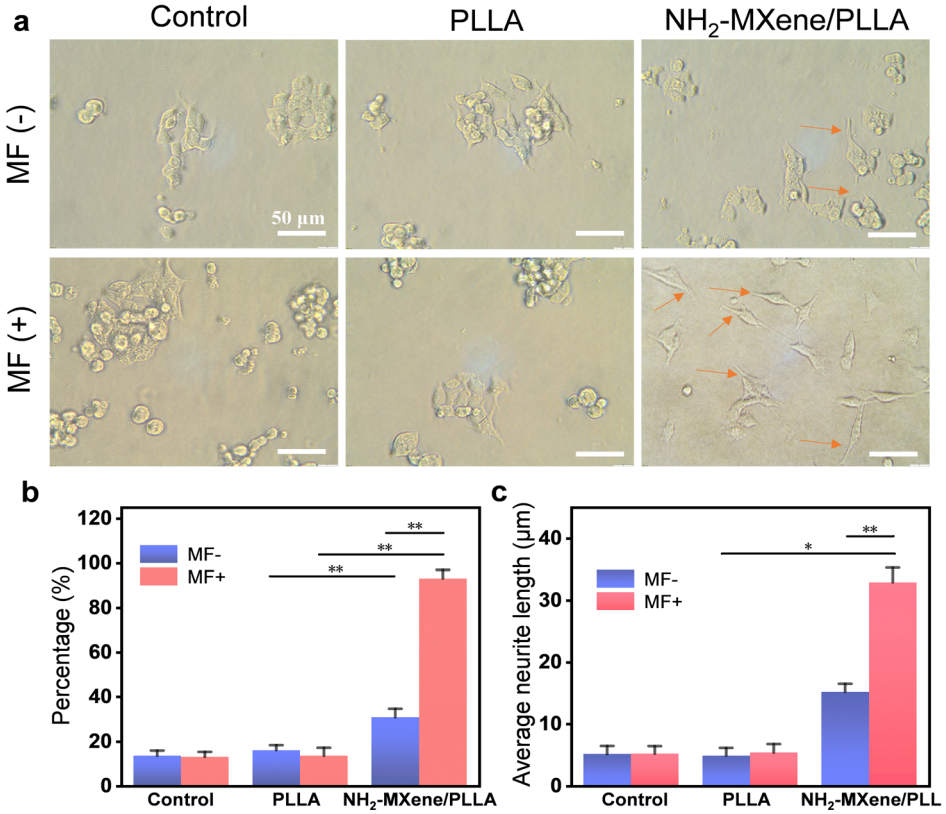

Fig. 7 (a) Optical microscopic images of PC12 cell differentiation on different substrates at day 5 with or without MF treatment, bar = 50 μm; (b) the percentages of PC12 differentiated and (c) average neurite length of differentiated neurons at day 5 with or without MF treatment. *$p < 0.05$ and **$p < 0.01$.

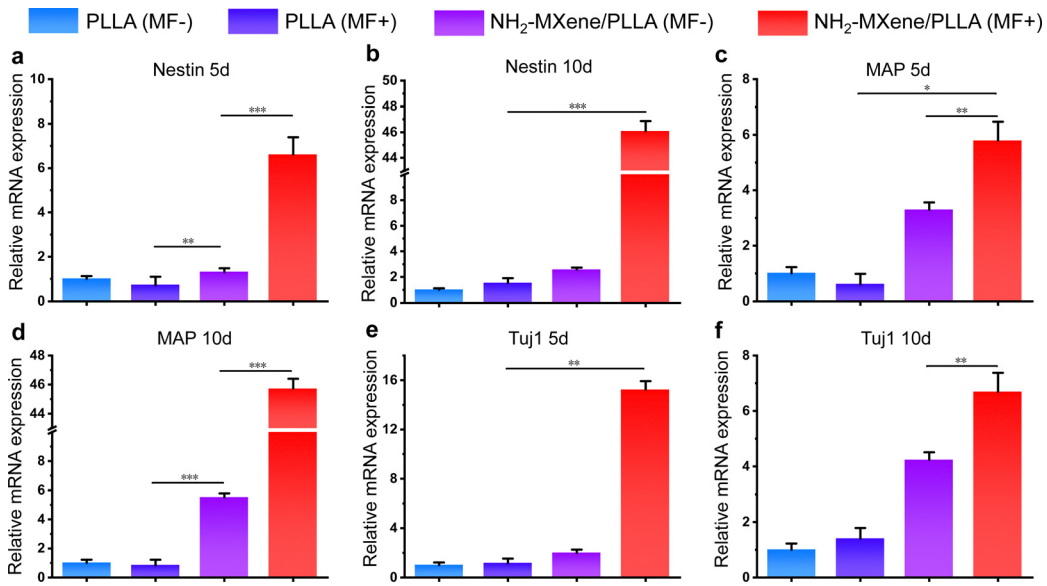

Fig. 8 qPCR analysis of the expression of neural-related genes (a and b) Nestin, (c and d) MAP2 and (e and f) Tuj1 for PC12 cells seeded on different substrates and cultured without or with a rotating magnetic field (300 rpm) for 5 and 10 days, respectively. *$p < 0.05$, **$p < 0.01$ and ***$p < 0.001$.

NH_2-MXene/PLLA driven by the rotating MF up-regulated the expression of differentiation-related mRNA to induce differentiation.[61–63] Therefore, the physical mechanism of electromagnetic induction promoting cell differentiation could be that the NH_2-MXene/PLLA conduit generated electrical signals driven by electromagnetic induction and the generated electrical signals promoted the differentiation of nerve cells by enhancing the mRNA expression of Nestin, MAP2 and Tuj1.

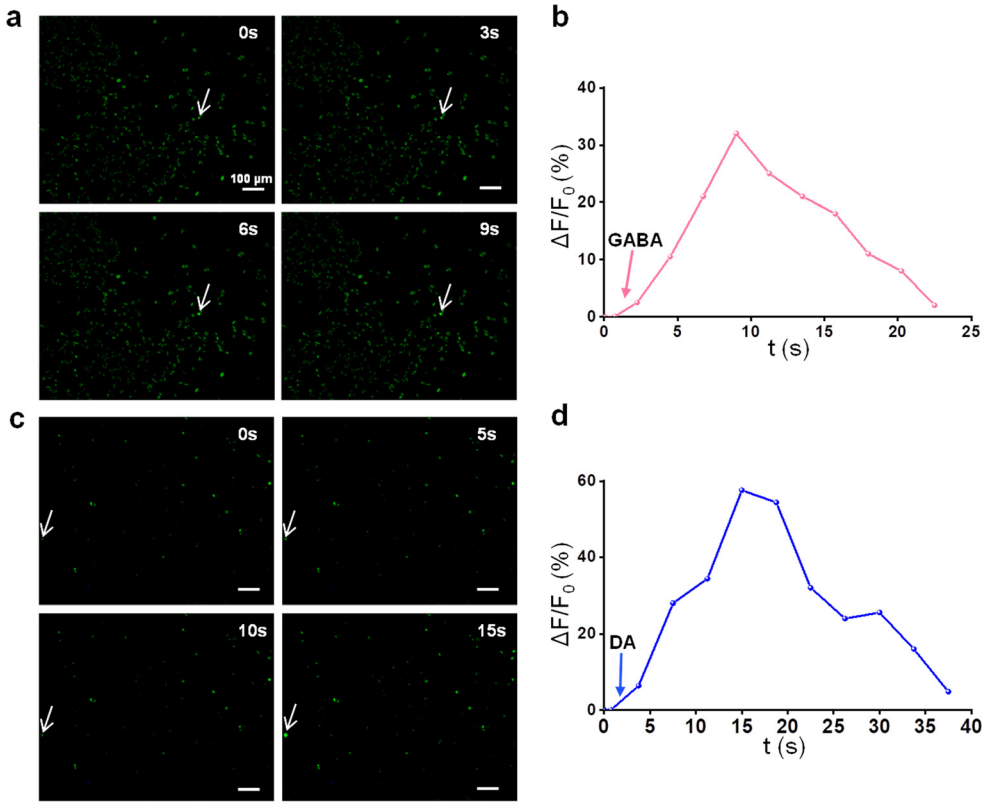

Fig. 9 Ca^{2+} fluorescence micrographs of cells responding (indicated by the white arrow) to (a) GABA and (c) DA; the relative intensity changes of cellular Ca^{2+} responding to (b) GABA and (d) DA.

3.8. Neuronal functional assay

One typical function of mature neurons was that they could respond to neurotransmitters for transmitting signals, and the calcium ion (Ca^{2+}) fluorescence probe could identify the function of mature neurons by detecting calcium sparks caused by neurotransmitter stimulation.[64] In this work, we used two neurotransmitters (inhibitory neurotransmitter GABA and excitatory neurotransmitter DA) to evaluate whether PC12 differentiated cells had the function of mature neurons mediated by the NH_2-MXene/PLLA conduit under the excitation of MF. GABA or DA could bind with receptors to change the membrane potential of nerve cells and generate nerve impulses. Only the nerve cells were mature, they could receive nerve impulses. The specific performance was that the permeability of Ca^{2+} in the presynaptic membrane increased, and a large amount of Ca^{2+} entered the synaptosome, forming a calcium spark.[65]

As shown in Fig. 9a, the Ca^{2+} fluorescence intensity of the initial cells was relatively low, whereas minor cells exhibited an enhancement of Ca^{2+} fluorescence after the addition of GABA. In addition, the long-term fluorescence curves revealed that Ca^{2+} fluorescence increased within a short time and then gradually reverted to the resting state level (Fig. 9b). The results indicated that calcium sparks were generated and proved that some cells were mature neurons with function.[66] Similarly, the Ca^{2+} fluorescence intensity of cells treated with DA showed the same change in trend as that of GABA (Fig. 9c and d). These collective results indicate that NH_2-MXene/PLLA conduits under the excitation of rotating MF promoted the PC12 cells to differentiate into mature neurons.[67]

4. Conclusions

In this study, a wireless electrical stimulation system based on electromagnetic induction was constructed by combining a rotating magnet with a conductive NH_2-MXene/PLLA conduit. The results showed that the conduits containing 10 wt% NH_2-MXene exhibited a favorable electrical conductivity of 8.44 S m^{-1} and generated a current of 10 μA under the excitation of a rotating magnetic field at 300 rpm. *In vitro* cell experiments confirmed that the generated electrical signals effectively enhanced nerve cell proliferation and differentiation, as evidenced by the increased PC12 differentiated percentages, boosted the average neurite length and up-regulated differentiation-related mRNA expression. Most significantly, the neuronal functional assay showed that the generated electrical stimulation promoted the differentiation of PC12 cells into the mature neuron. Overall, this work provides a potential wireless electrical stimulation strategy for nerve repair.

Conflicts of interest

There are no conflicts to declare.

Acknowledgements

This study was supported by the following funds: the Natural Science Foundation of China (51935014, 52165043, 52105352, 82072084), the JiangXi Provincial Natural Science Foundation of China (20224ACB204013), the Technology Innovation Platform Project of Shenzhen Institute of Information Technology 2020 (PT2020E002), Guangdong Province Precision Manufacturing and Intelligent production education Integration Innovation Platform (2022CJPT019), Shccig-Qinling Program (2022360702014891), The Opening Project of State Key Laboratory of Polymer Materials Engineering (Sichuan University) (sklpme2020-4-15), China Postdoctoral Science Foundation (2021M690121), Project supported by the Research Foundation of Education Bureau of Hunan Province, China (Grant No. 21A0247), and National First-Class Disciplinary Construction Project of Hunan Province in Traditional Chinese Medicine (Grant No. 2022ZYX24).

References

1 B. Ferrigno, R. Bordett, N. Duraisamy, J. Moskow, M. R. Arul, S. Rudraiah, S. P. Nukavarapu, A. T. Vella and S. G. Kumbar, Bioactive polymeric materials and electrical stimulation strategies for musculoskeletal tissue repair and regeneration, *Bioact. Mater.*, 2020, **5**, 468–485.

2 Y. Qian, Y. Cheng, J. Cai, X. Zhao, Y. Ouyang, W.-E. Yuan and C. Fan, Advances in electrical and magnetic stimulation on nerve regeneration, *Regener. Med.*, 2019, **14**, 969–979.

3 C. Dong, F. Qiao, W. Hou, L. Yang and Y. Lv, Graphene-based conductive fibrous scaffold boosts sciatic nerve regeneration and functional recovery upon electrical stimulation, *Appl. Mater. Today*, 2020, **21**, 100870.

4 C. Wu, A. Liu, S. Chen, X. Zhang, L. Chen, Y. Zhu, Z. Xiao, J. Sun, H. Luo and H. Fan, Cell-laden electroconductive hydrogel simulating nerve matrix to deliver electrical cues and promote neurogenesis, *ACS Appl. Mater. Interfaces*, 2019, **11**, 22152–22163.

5 X. Li, W. Yang, H. Xie, J. Wang, L. Zhang, Z. Wang and L. Wang, CNT/sericin conductive nerve guidance conduit promotes functional recovery of transected peripheral nerve injury in a rat model, *ACS Appl. Mater. Interfaces*, 2020, **12**, 36860–36872.

6 H. Sheng, X. Zhang, J. Liang, M. Shao, E. Xie, C. Yu and W. Lan, Recent advances of energy solutions for implantable bioelectronics, *Adv. Healthcare Mater.*, 2021, **10**, 2100199.

7 J. Pang, S. Peng, C. Hou, X. Wang, T. Wang, Y. Cao, W. Zhou, D. Sun, K. Wang and M. H. Rümmeli, Applications of MXenes in human-like sensors and actuators, *Nano Res.*, 2022, 1–29.

8 E. Mostafavi and S. Iravani, Mxene-graphene composites: A perspective on biomedical potentials, *Nano-Micro Lett.*, 2022, **14**, 130.

9 Y. Cao, P. Qu, C. Wang, J. Zhou, M. Li, X. Yu, X. Yu, J. Pang, W. Zhou and H. Liu, Epitaxial Growth of Vertically Aligned Antimony Selenide Nanorod Arrays for Heterostructure Based Self-Powered Photodetector, *Adv. Opt. Mater.*, 2022, **10**, 2200816.

10 J. Tang, C. Wu, Z. Qiao, J. Pi, Y. Zhang, F. Luo, J. Sun, D. Wei and H. Fan, A photoelectric effect integrated scaffold for the wireless regulation of nerve cellular behavior, *J. Mater. Chem. B*, 2022, **10**, 1601–1611.

11 Y. Cheng, Y. Xu, Y. Qian, X. Chen, Y. Ouyang and W.-E. Yuan, 3D structured self-powered PVDF/PCL scaffolds for peripheral nerve regeneration, *Nano Energy*, 2020, **69**, 104411.

12 G. Giuliani, A general law for electromagnetic induction, *EPL*, 2008, **81**, 60002.

13 J. Pang, B. Chang, H. Liu and W. Zhou, Potential of MXene-based heterostructures for energy conversion and storage, *ACS Energy Lett.*, 2021, **7**, 78–96.

14 J. Pang, R. G. Mendes, A. Bachmatiuk, L. Zhao, H. Q. Ta, T. Gemming, H. Liu, Z. Liu and M. H. Rummeli, Applications of 2D MXenes in energy conversion and storage systems, *Chem. Soc. Rev.*, 2019, **48**, 72–133.

15 W. Yang, B. Huang, L. Li, K. Zhang, Y. Li, J. Huang, X. Tang, T. Hu, K. Yuan and Y. Chen, Covalently sandwiching MXene by conjugated microporous polymers with excellent stability for supercapacitors, *Small Methods*, 2020, **4**, 2000434.

16 Y. Wang and Y. Wang, Recent progress in MXene layers materials for supercapacitors: High-performance electrodes, *SmartMat*, 2023, **4**, e1130.

17 A. Feng, Y. Yu, Y. Wang, F. Jiang, Y. Yu, L. Mi and L. Song, Two-dimensional MXene Ti_3C_2 produced by exfoliation of Ti_3AlC_2, *Mater. Des.*, 2017, **114**, 161–166.

18 S. De, S. Acharya, S. Sahoo, J.-J. Shim and G. C. Nayak, From 0D to 3D MXenes: their diverse syntheses, morphologies and applications, *Mater. Chem. Front.*, 2022, **6**, 818.

19 S. De, S. Acharya, S. Sahoo and G. C. Nayak, Current trends in MXene research: properties and applications, *Mater. Chem. Front.*, 2021, **5**, 7134–7169.

20 G. Zhang, T. Wang, Z. Xu, M. Liu, C. Shen and Q. Meng, Synthesis of amino-functionalized $Ti_3C_2T_x$ MXene by alkalization-grafting modification for efficient lead adsorption, *Chem. Commun.*, 2020, **56**, 11283–11286.

21 G. Ruano, M. Pedano, M. Albornoz, J. Fuhr, M. Martiarena and G. Zampieri, Deprotonation of the amine group of Glyphosate studied by XPS and DFT, *Appl. Surf. Sci.*, 2021, **567**, 150753.

22 H. Riazi, M. Anayee, K. Hantanasirisakul, A. A. Shamsabadi, B. Anasori, Y. Gogotsi and M. Soroush, Surface modification of a MXene by an aminosilane coupling agent, *Adv. Mater. Interfaces*, 2020, **7**, 1902008.

23 J. K. Oh, Y. Yegin, F. Yang, M. Zhang, J. Li, S. Huang, S. V. Verkhoturov, E. A. Schweikert, K. Perez-Lewis and E. A. Scholar, The influence of surface chemistry on the kinetics and thermodynamics of bacterial adhesion, *Sci. Rep.*, 2018, **8**, 1–13.

24 P. N. Fotsing, N. Bouazizi, E. D. Woumfo, N. Mofaddel, F. Le Derf and J. Vieillard, Investigation of chromate and nitrate removal by adsorption at the surface of an amine-modified cocoa shell adsorbent, *J. Environ. Chem. Eng.*, 2021, **9**, 104618.

25 W. Ren, L. Xiong, G. Nie, H. Zhang, X. Duan and S. Wang, Insights into the electron-transfer regime of peroxydisulfate activation on carbon nanotubes: the role of oxygen functional groups, *Environ. Sci. Technol.*, 2019, **54**, 1267–1275.

26 J. Fu, L. Li, J. M. Yun, D. Lee, B. K. Ryu and K. H. Kim, Two-dimensional titanium carbide (MXene)-wrapped sisal-Like $NiCo_2S_4$ as positive electrode for High-performance hybrid pouch-type asymmetric supercapacitor, *Chem. Eng. J.*, 2019, **375**, 121939.

27 R. Sun, H. B. Zhang, J. Liu, X. Xie, R. Yang, Y. Li, S. Hong and Z. Z. Yu, Highly conductive transition metal carbide/carbonitride (MXene)@ polystyrene nanocomposites fabricated by electrostatic assembly for highly efficient electromagnetic interference shielding, *Adv. Funct. Mater.*, 2017, **27**, 1702807.

28 S. Dhivya and K. Kalaichelvi, UV-Vis spectroscopic and FTIR analysis of Sarcostemma brevistigma, wight. and arn, *Int. J. Tradit. Herb. Med.*, 2017, **9**, 46–49.

29 Z. Zhang, Y. Chen, C. Hu, C. Zuo, P. Wang, W. Chen and T. Ao, Efficient removal of tetracycline by a hierarchically porous ZIF-8 metal organic framework, *Environ. Res.*, 2021, **198**, 111254.

30 S. Tang, J. Yang, L. Lin, K. Peng, Y. Chen, S. Jin and W. Yao, Construction of physically crosslinked chitosan/sodium alginate/calcium ion double-network hydrogel and its application to heavy metal ions removal, *Chem. Eng. J.*, 2020, **393**, 124728.

31 P. Feng, R. Zhao, W. Tang, F. Yang, H. Tian, S. Peng, H. Pan and C. Shuai, Structural and functional adaptive artificial bone: materials, fabrications and properties, *Adv. Funct. Mater.*, 2023, 2214726.

32 C. Shuai, S. Zhong, Y. Shuai, W. Yang, S. Peng and C. He, Accelerated anode and cathode reaction due to direct electron uptake and consumption by manganese dioxide and titanium dioxide composite cathode in degradation of iron composite, *J. Colloid Interface Sci.*, 2023, **632**, 95–107.

33 S. Santoni, S. G. Gugliandolo, M. Sponchioni, D. Moscatelli and B. M. Colosimo, 3D bioprinting: current status and trends—a guide to the literature and industrial practice, *Bio-Des. Manuf.*, 2021, 1–29.

34 Y. Yang, C. Ling, Y. Li, S. Peng, D. Xie, L. Shen, Z. Tian and C. Shuai, Microstructure development and biodegradation behavior of additively manufactured Mg-Zn-Gd alloy with LPSO structure, *J. Mater. Sci. Technol.*, 2023, **144**, 1–14.

35 A. Magaz, A. Faroni, J. E. Gough, A. J. Reid, X. Li and J. J. Blaker, Bioactive silk-based nerve guidance conduits for augmenting peripheral nerve repair, *Adv. Healthcare Mater.*, 2018, **7**, 1800308.

36 X. Gan, G. Fei, J. Wang, Z. Wang, M. Lavorgna and H. Xia, Powder quality and electrical conductivity of selective laser sintered polymer composite components, *Struct. Prop. Addit. Manuf. Polym. Compon.*, 2020, 149–185.

37 H. Liao, X. Guo, P. Wan and G. Yu, Conductive MXene nanocomposite organohydrogel for flexible, healable, low-temperature tolerant strain sensors, *Adv. Funct. Mater.*, 2019, **29**, 1904507.

38 F. Qi, R. Liao, Y. Shuai, H. Pan, G. Qian, S. Peng and C. Shuai, A conductive network enhances nerve cell response, *Addit. Manuf.*, 2022, **52**, 102694.

39 J. Zhou, D. Meng, T. Yang, X. Zhang, Z. Tang, Y. Cao, J. Ni, J. Zhang, Z. Hu and J. Pang, Enhanced charge carrier transport via efficient grain conduction mode for Sb_2Se_3 solar cell applications, *Appl. Surf. Sci.*, 2022, **591**, 153169.

40 Y. Cao, C. Liu, J. Jiang, X. Zhu, J. Zhou, J. Ni, J. Zhang, J. Pang, M. H. Rummeli and W. Zhou, Theoretical insight into high-efficiency triple-junction tandem solar cells via the band engineering of antimony chalcogenides, *Solar RRL*, 2021, **5**, 2000800.

41 Y. Cao, C. Liu, T. Yang, Y. Zhao, Y. Na, C. Jiang, J. Zhou, J. Pang, H. Liu and M. H. Rummeli, Gradient bandgap modification for highly efficient carrier transport in antimony sulfide-selenide tandem solar cells, *Sol. Energy Mater. Sol. Cells*, 2022, **246**, 111926.

42 K. Zhang, J. Li, J. Jin, J. Dong, L. Li, B. Xue, W. Wang, Q. Jiang and Y. Cao, Injectable, anti-inflammatory and conductive hydrogels based on graphene oxide and diacerein-terminated four-armed polyethylene glycol for spinal cord injury repair, *Mater. Des.*, 2020, **196**, 109092.

43 P. Di Benedetto, A. Casati, L. Bertini and G. Fanelli, Posterior subgluteal approach to block the sciatic nerve: description of the technique and initial clinical experiences, *Eur. J. Anaesthesiol.*, 2002, **19**, 682–686.

44 M. E. Everett and A. D. Chave, On the physical principles underlying electromagnetic induction, *Geophysics*, 2019, **84**, W21–W32.

45 A. T. Nguyen, S. Mattiassi, M. Loeblein, E. Chin, D. Ma, P. Coquet, V. Viasnoff, E. H. T. Teo, E. L. Goh and E. K. Yim, Human Rett-derived neuronal progenitor cells in 3D graphene scaffold as an in vitro platform to study the effect of electrical stimulation on neuronal differentiation, *Biomed. Mater.*, 2018, **13**, 034111.

46 M. Yang, L. Yang, S. Peng, F. Deng, Y. Li, Y. Yang and C. Shuai, Laser additive manufacturing of zinc: formation quality, texture, and cell behavior, *Bio-Des. Manuf.*, 2022, 1–18.

47 F. Qi, Z. Wang, L. Yang, H. Li, G. Chen, S. Peng, S. Yang and C. Shuai, A collaborative CeO2@ metal-organic framework nanosystem to endow scaffolds with photodynamic antibacterial effect, *Mater. Today Chem.*, 2023, **27**, 101336.

48 G. Qian, L. Zhang, Y. Shuai, X. Wu, Z. Zeng, S. Peng and C. Shuai, 3D-printed CuFe2O4-MXene/PLLA antibacterial tracheal scaffold against implantation-associated infection, *Appl. Surf. Sci.*, 2023, **614**, 156108.

49 G. Qian, J. Wang, L. Yang, Z. Zeng, Z. Zhao, S. Peng and C. Shuai, A pH-responsive CaO2@ ZIF-67 system endows a scaffold with chemodynamic therapy properties, *J. Mater. Sci.*, 2023, 1–15.

50 R. Liu, X. Huang, X. Wang, X. Peng, S. Zhang, Y. Liu, D. Yang and Y. Min, Electrical stimulation mediated the neurite outgrowth of PC-12 cells on the conductive polylactic acid/reduced graphene oxide/polypyrrole composite nanofibers, *Appl. Surf. Sci.*, 2021, **560**, 149965.

51 R. Liu, Z. Xu, C. Zhao, S. Zhang, H. Zhou, L. Zhou, Y. Liu and Y. Min, Mediate neurite outgrowth of PC-12 cells using polypyrrole-assisted laser-induced graphene flexible composite electrodes combined with electrical stimulation, *Eur. Polym. J.*, 2022, **181**, 111634.

52 J. Zan, Y. Shuai, J. Zhang, J. Zhao, B. Sun and L. Yang, Hyaluronic acid encapsulated silver metal organic framework for the construction of a slow-controlled bifunctional nanostructure: Antibacterial and anti-inflammatory in intrauterine adhesion repair, *Int. J. Biol. Macromol.*, 2023, 123361.

53 P. Feng, S. Shen, Y. Shuai, S. Peng, C. Shuai and S. Chen, PLLA grafting draws GO from PGA phase to the interface in PLLA/PGA bone scaffold owing enhanced interfacial bonding, *Sustainable Mater. Technol.*, 2023, e00566.

54 B. Sun, Z. Zhou, T. Wu, W. Chen, D. Li, H. Zheng, H. El-Hamshary, S. S. Al-Deyab, X. Mo and Y. Yu, Development of nanofiber sponges-containing nerve guidance conduit for peripheral nerve regeneration in vivo, *ACS Appl. Mater. Interfaces*, 2017, **9**, 26684–26696.

55 A. F. Weidema, T. N. Kropacheva, J. Raap and D. L. Ypey, Membrane Permeabilization of a Mammalian Neuroendocrine Cell Type (PC12) by the Channel-Forming Peptides Zervamicin, Alamethicin, and Gramicidin, *Chem. Biodiversity*, 2007, **4**, 1347–1359.

56 Z. Wang, Y. Zhang, L. Wang, Y. Ito, G. Li and P. Zhang, Nerve implants with bioactive interfaces enhance neurite outgrowth and nerve regeneration in vivo, *Colloids Surf., B*, 2022, **218**, 112731.

57 Y.-S. Hsiao, Y.-H. Liao, H.-L. Chen, P. Chen and F.-C. Chen, Organic photovoltaics and bioelectrodes providing electrical stimulation for PC12 cell differentiation and neurite outgrowth, *ACS Appl. Mater. Interfaces*, 2016, **8**, 9275–9284.

58 W. Jing, Y. Zhang, Q. Cai, G. Chen, L. Wang, X. Yang and W. Zhong, Study of electrical stimulation with different electric-field intensities in the regulation of the differentiation of PC12 cells, *ACS Chem. Neurosci.*, 2018, **10**, 348–357.

59 H. q Zhang, D. w Lan, X. Li, Z. Li and F. Y. Dai, Conductive and antibacterial scaffold with rapid crimping property for application prospect in repair of peripheral nerve injury, *J. Appl. Polym. Sci.*, 2023, **140**, e53426.

60 S. Song and P. M. George, Conductive polymer scaffolds to improve neural recovery, *Neural Regener. Res.*, 2017, **12**, 1976.

61 N. C. Tsai, J. W. She, J. G. Wu, P. Chen, Y. S. Hsiao and J. Yu, Poly(3, 4-ethylenedioxythiophene) polymer composite bioelectrodes with designed chemical and topographical cues to manipulate the behavior of pc12 neuronal cells, *Adv. Mater. Interfaces*, 2019, **6**, 1801576.

62 S. Shrestha, B. K. Shrestha, O. K. Joong, C. H. Park and C. S. Kim, Para-substituted sulfonic acid-doped protonated emeraldine salt nanobuds: a potent neural interface targeting PC12 cell interactions and promotes neuronal cell differentiation, *Biomater. Sci.*, 2021, **9**, 1691–1704.

63 B. S. Eftekhari, M. Eskandari, P. A. Janmey, A. Samadikuchaksaraei and M. Gholipourmalekabadi, Surface topography and electrical signaling: single and synergistic effects on neural differentiation of stem cells, *Adv. Funct. Mater.*, 2020, **30**, 1907792.

64 Z. Guo, C. Sun, H. Yang, H. Gao, N. Liang, J. Wang, S. Hu, N. Ren, J. Pang and J. Wang, Regulation of Neural Differentiation of ADMSCs using Graphene-Mediated Wireless-Localized Electrical Signals Driven by Electromagnetic Induction, *Adv. Sci.*, 2022, **9**, 2104424.

65 Y. Dunant and A. Bloc, Low-and high-affinity reactions in rapid neurotransmission, *Neurochem. Res.*, 2003, **28**, 659–665.

66 L. Liang, C. Liu, P. Cai, S. Han, R. Zhang, N. Ren, J. Wang, J. Yu, S. Shang and W. Zhou, Highly specific differentiation of MSCs into neurons directed by local electrical stimuli triggered wirelessly by electromagnetic induction nanogenerator, *Nano Energy*, 2022, **100**, 107483.

67 H. Yang, Y. Su, Z. Sun, B. Ma, F. Liu, Y. Kong, C. Sun, B. Li, Y. Sang and S. Wang, Gold Nanostrip Array-Mediated Wireless Electrical Stimulation for Accelerating Functional Neuronal Differentiation, *Adv. Sci.*, 2022, **9**, 2202376.